

Automatic crack detection on 2D pavement images: An algorithm based on minimal path selection

Rabih Amhaz¹, Sylvie Chambon², Jérôme Idier³, *Member, IEEE*, and Vincent Baltazart¹

Abstract—This paper proposes a new algorithm for automatic crack detection from 2D pavement images. It strongly relies on the localization of minimal paths within each image, a path being a series of neighboring pixels and its score being the sum of their intensities. The originality of the approach stems from the proposed way to select a set of minimal paths and the two post-processing steps introduced to improve the quality of the detection. Such an approach is a natural way to take account of both the photometric and geometric characteristics of pavement images. An intensive validation is performed on both synthetic and real images (from five different acquisition systems), with comparisons to five existing methods. The proposed algorithm provides very robust and precise results in a wide range of situations, in a fully unsupervised manner, which is beyond the current state-of-the-art.

Index Terms—Crack detection, minimal path, Dijkstra algorithm, non destructive control, road surface condition.

I. INTRODUCTION

SURVEYS of pavement condition is an important task to insure road safety. In many countries, pavement distress detection is considered as an essential step for road surface inspection. The objective is to detect surface distresses, like raveling and cracking, in order to plan effective road maintenance and to afford a better sustainability of the pavement structure. The most common type of surface distress is cracking. Human visual inspection has been gradually replaced by automatic data collection at traffic speed using both area and line scan cameras [1]. Off-line processing techniques have been then developed for surface condition monitoring as a support of human visual control. Readers can find a brief history of the imaging devices in [2]. CCD, Charge-Coupled Device, acquisition techniques provide information on the presence of cracks through the pixel intensities (pixels corresponding to cracks being generally of dark intensity). 3D imaging technology has emerged in the past years and gives the imaging system to detect distresses thanks to the elevation data. In the paper, we concentrate on crack detection by processing 2D pavement images with the prospect to generalize the proposed method to the latest 3D imaging technologies.

Full automation of crack monitoring is a challenging image processing problem, because in most cases the cracks appear

as thin, irregular lines, buried into a strong, textured noise. Indeed, only few of the existing methods are fully unsupervised [3]

Photometry-based approaches – Quite different principles have been adopted to tackle the problem. The most basic methods are based on the sole photometric information, *i.e.*, they decide whether each pixel belongs to a crack according to a simple thresholding operation. Some methods determine the threshold value in a global way [4], and other at a local scale, *e.g.*, in small patches, with adaptive thresholding [5] or by hysteresis [6]. To determine the threshold, many optimisation approaches can be involved from the simplest one based on Otsu algorithm [7] to more sophisticated ones, like fuzzy logic based techniques [8] and genetic algorithms [9]. All these approaches are of limited efficiency, since the pixels corresponding to cracks cannot be well separated from the other pixels by a simple thresholding operation [10]. Photometry-based methods can also involve a supervised learning step. For instance, the training of a neural network [11], a Bayesian classifier [12], an Adaboost classifier [13], or the estimation of the parameters of Gaussian mixture [14] are often considered to solve this classification problem. However, such photometry-based methods suffer from one important drawback in our context: the need of a supervised training stage.

Introduction of geometric constraints – More efficient methods incorporate spatial processing steps involving groups of pixels at a local scale. For instance, mathematical morphology based methods consider dilation and erosion operators to reduce the discontinuities within the crack pattern and to remove false detections [15], [5]. However, the automatic implementation of the latter methods remains difficult because of the large amount of parameters to tune. Based on the fact that cracks can have different width and size, multi-scale analysis with watersheds [16], wavelet decomposition [17] have been intensively used but the main difficulty is to select the right scale for identifying cracks or how to combine the detections at multi-scale to compute the final decision.

Photometry and geometry-based approaches – Advanced methods introduce higher-level geometrical information on the topology of cracks combined with the photometric information. Cracks are then considered as sets of contiguous pixels of low intensities. For instance, the Markov based method proposed in [18], [10] favours the continuity between neighbouring crack pixels using a statistical approach. However, it is a computationally intensive method, and it relies on statistical parameter values that must be tuned in a supervised manner. Let us remark that the crack detection problem from pavement images shares some common points with other

¹ LUNAM Université, IFSTTAR, 44344 Bouguenais, France.

² Université de Toulouse, INP-ENSEEIHT, IRIT, 31071 Toulouse, France.

³ LUNAM Université, IRCCyN, UMR CNRS 6597, Ecole Centrale de Nantes, 44321 Nantes, France.

This work was partially supported by the French Région Pays de la Loire. This work may contribute to the technical group TG3 (Advanced measurement systems for crack characterization) of the RILEM Technical Committee 241-MCD on Mechanisms of Cracking and Debonding in Asphalt and Composite Pavements.

tracking problems, such as fibre tracking from diffusion MRI images, or object contour tracking for image segmentation. Some authors have exploited these similarities to propose crack detection methods using a tensor voting strategy [19], on active or geodesic contour approach [20], [5], for instance. In the latter case, a crucial step of the methods relies on a *minimal path* principle (also referred to as *shortest path* principle) that is also shared by other recent contributions [21], [22].

Minimal path based methods – Generally speaking, the minimal path problem consists in finding best paths between pairs of nodes in a graph, with respect to a criterion defined as a cumulated cost along the paths. In the context of image processing, the cost usually combines two terms. The first one accounts for the pixel intensities along the path, and the second one locally evaluates the regularity of the path [23], [24]. The two latter terms are often called an external and an internal energy, respectively, and also as a fidelity-to-data term and a regularizing term.

Efficient applications of the minimal path principle to several image processing problems are made possible because fast algorithms exist to compute the solutions, such as Dijkstra's algorithm [25] and the fast marching algorithm [26], the latter being specifically suited to minimize costs involving an internal energy based on the length of the path. Thanks to such algorithms, it is possible to take relatively high-level geometrical information into account, while maintaining moderate computing time and memory requirement. However, the direct application of the minimal path principle requires that some information be known in advance, such as the two endpoints of each path to be detected. Unfortunately, such a prior knowledge is not available in a fully unsupervised context. Worse than that, cracks are not simple lines. They may appear as complex networks of unknown geometry. To overcome both difficulties, several recent methods share a common overall structure [20], [21], [19], [23], [22]:

- In a first step, some of the darkest pixels are selected as the best candidates to belong to the crack structure.
- In a second step, pairs of preselected pixels are considered as endpoints and minimal paths joining them are built with a view to track the whole structure of the cracks.

At the first step, some contributions proceed according to a manual procedure [23]. Others rely in a more automatic way [20], [22]. Finally, [21] considers that every pixel is a potential endpoint. At the second step, [20], [19] use a regularization term to favour the smoothness of the trajectory, while [21], [22] only consider the cumulated pixel intensities along the paths, without any internal energy term. In this paper, we adopt the latter approach, because we consider that the shape of pavement cracks is too irregular to be well described by any internal energy term favouring smooth curves.

Contributions – Indeed, it is a distinctive contribution of the present paper (shared by our early version [22]) to develop a crack detection method that is only based on the photometry and on a minimal assumption that pixels belonging to the cracks form continuous paths of arbitrary shape. In particular, a difference between [21] and ours is that the former assumes that each crack is organized along a preferred direction, so that it can be tracked using a faster algorithm

than Dijkstra's algorithm for all possible pairs of endpoints. In contrast, we do not make any restriction on the shape of the cracks, while being more selective at the initial stage of electing potential pairs of endpoints. Additionally, our method incorporates two post-processing steps, where the currently detected paths are merged, and some pixels are added to the crack or removed, depending on their position and on their photometry. In particular, the resulting detected cracks gain a certain thickness, whereas the minimal path stage only provides one pixel thick paths.

Another distinctive feature of the proposed method is its fully unsupervised character at all stages, including the initial stage of endpoint selection. We emphasize here that all the tests presented in the paper to illustrate the efficiency of the method have been performed with fixed values for all the parameters.

Organisation of the paper – The next section introduces further details on the minimal path principle and on its existing applications to road crack detection. Section III contains our own contribution, under the form of the three-stage method sketched above, where the minimal path principle is the central part of the processing chain and two post-processing steps to refine the detection and to estimate the width of the cracks. Section V proposes a performance study, along a protocol introduced in Section IV. It includes a comparison with five existing methods, and both synthetic and real images are considered. Section VI contains the main perspectives of the present contribution.

II. EXISTING MINIMAL PATH APPROACHES

A. Minimal paths in graph theory

In graph theory, finding shortest paths consists in estimating a path between two vertices such that it minimizes a cost that is usually the sum of the weights of each edge included in the path. In this paper we have chosen the term minimal path instead of shortest path because it better corresponds to what is done, *i.e.*, the paths have to minimize a cost that does not take into account a geometric distance. In the rest of the paper, we always use the term minimal path.

Algorithms for finding minimal paths have been efficiently used for transportation networks, high performance communication, fault tolerant routing [27]. By considering images as connected graph of pixels, minimal path extraction has been used for a number of applications in image processing such as segmentation or medical images [28], road extraction in satellite images [29] or object boundary extraction [30].

For using minimal path estimation algorithms, these two important elements have to be chosen:

- 1) The used **cost function** depends on the weight of each edge. It should be designed so that good solutions have a low cost while poor solutions have high cost. In image processing, most of the cost functions are based on grey levels or colours. Moreover, many techniques include a regularization term in order to minimize the distance, the regularity of the path, the length of the path [23], [24]. These terms are really appropriate in applications such as detecting blood vessel in medical imagery because

the object to detect have a regular shape and a constraint length. In the case of crack detection, these constraints are not really appropriate because the shape of the cracks is more chaotic.

- 2) The **optimization** approach to find the path that minimizes this cost – The most famous methods are the Dijkstra algorithm [25] and the fast marching approach [26].

The way to design the cost influences the optimization approach that is chosen and *vice versa*. The rest of the paper focuses on using these costs and optimization approaches for crack detection.

B. Cost and optimization for road crack detection

Pavement images are highly textured images and cracks are long dark filaments that can be assimilated to perceptually salient curves. It naturally leads to search for a path composed of dark pixels [27]. In the context of active contours, the goal is to find a curve that fits an object or a region by iteratively minimizing a cost or energy function, E , of the curve \mathcal{C} , defined by [31]:

$$E(\mathcal{C}) = \int_0^L \left(w_1 \|\mathcal{C}'(v)\|^2 + w_2 \|\mathcal{C}''(v)\|^2 + \mathcal{P}(\mathcal{C}(v)) \right) dv, \quad (1)$$

where $c(v)$ represents a curve drawn on a 2D image, $[0, L]$ its domain of definition, and L the length of the curve. The two first terms represent the *internal forces* (regularity of the curve) based on first and second derivatives with w_1, w_2 the weights of each of these two parts. The third term is the *external force*. Here, we consider an external force based on grey levels. Moreover, the first two terms favor smooth curves, whereas the shape of the cracks are not smooth in general. Therefore, we propose a simple cost function c that only incorporates an external force:

$$c(p_{ij}) = \sum_{m=i}^j I(m), \quad (2)$$

where x_i is the source point, x_j the destination point, and m is a pixel of the path. In [20], an additional regularization term was considered. Here, we advocate that using the cost (2) is more natural to recover crack patterns as series of connected pixels with arbitrary shapes and lengths.

The minimization of a separable cost such as (2) is a so called minimal path finding problem between two points. The reference algorithm to solve such a problem is the Dijkstra algorithm which has a linear overall complexity as a function of the problem size [?]. Owing to the simplicity of its structure, we have retained this algorithm to minimize (2).

In the particular context of road crack detection, a difficulty is that we do not know in advance the endpoints of the minimal paths to detect. Potentially, a minimal path could be estimated between each pair of pixels of the image, in order to select only the best ones at a subsequent step. However, the computational time to solve so many minimal paths problems using a Dijkstra type alggorithm is clearly out of reach. As a consequence, a strategy must be adopted to reduce the computational time. Two types of solutions have been proposed in the recent literature. Both of them introduce some constraints on the estimation of the paths, as explained below.

C. Computation strategies for minimal paths

- 1) **Introduction of constraints on the optimization process:**

Most of the proposed constraints affect the geometry of the paths: disjointness, ordering, spacing, length, smoothness [27]. With the advantage of being less selective for the endpoints, [21], [?] propose to compute the minimal path from each pixel of the image with a directional constraint (only four orientations are considered) and a fixed distance (typically chosen between 4 and 32 pixels). The main feature of the approach in [21], [?] is to consider that if one orientation gives different grey level distribution than the other orientations, the pixel is probably inside a crack. Consequently, individual pixels are selected rather than paths, with the drawback that the continuity along the cracks is not necessarily preserved. Moreover, such an approach is not able to detect cracks with fast variations of orientation.

- 2) **Selection of a subset of sources and destinations**

based on manual selection [23] or automatic selection of points of interest [20]. In the concerned application, a fully automatic process is by far preferable than a manual selection version. Moreover, the latter approach may be too selective, since the detected points of interest do not necessarily cover all the crack, leading to an incomplete segmentation. In [22], the possible endpoints are chosen among the pixels that correspond to local maxima of intensity. Then, minimal paths are computed at the local level without direction or length constraints.

In the following section, a refined version of the strategy proposed in [22] is presented.

III. MINIMAL PATH SELECTION FOR AUTOMATIC CRACK DETECTION

A. General algorithm

The proposed method is called Minimal Path Selection (MPS) algorithm. It is mainly based on the principle that minimal path within a crack reaches a lower cost function than any other minimal path within the image background. The image is analysed from a local to a global point of view: at a local level, significant pixels are selected as endpoints and minimal paths between endpoint pairs are computed without neither direction nor length constraints. Then, at a global level, a subset of minimal paths of lowest costs is selected. We suppose that images have no lighting defaults, *i.e.*, halos or a non-uniform lighting are removed by a pre-processing step, if needed. Two post-processing steps are also performed. The first one allows to remove some residual artefacts. Finally, the width of the crack is locally estimated.

Fig. 1 provides an illustration of the successive operations. Let us stress that the three core elements and the two post-processing steps of the method are all based on pixel intensities, which makes MPS a coherent, fully data driven method.

B. Core steps of MPS

The three core steps of the proposed MPS algorithm are summed up in Fig. 2 and are detailed below.

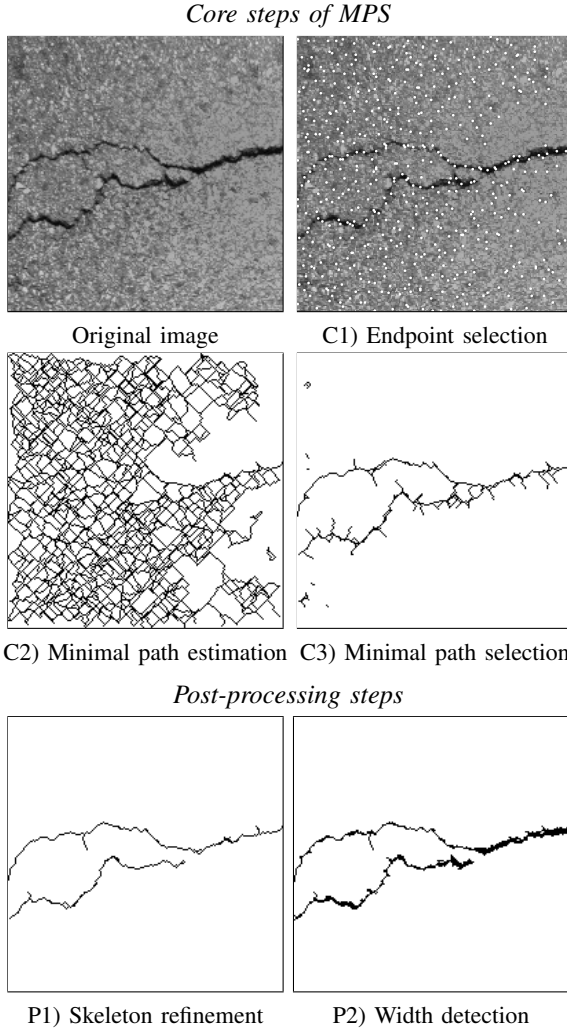


Fig. 1. Illustration of the five steps of the MPS method.

C1) Endpoint selection \mathcal{E} : Our goal is to select a significant proportion of the endpoints e_i inside the cracks. A first simple step is to partition the image into small square sub-images and to retain the one darkest pixel m_i in each of them. Some of the candidates are then removed if their intensity is above a threshold of the form $T_e = \mu - k_e\sigma$, where μ and σ are the mean and the standard deviation of the whole image. See Subsection V-A for more details about the choice of the sub-image dimension P and of the coefficient k_e .

C2) Minimal path estimation p_{ij} :

Dijkstra algorithm [25] is used to compute the minimal paths p_{ij} between each pair (e_i, e_j) of endpoints using equation (2) for the minimization. Following the first step of the algorithm, the endpoint e_i is surrounded by eight endpoints e_j at most. An important aspect is that by using this algorithm and the cost defined in (2), there is no constraint on the shape and the length of the paths.

C3) Minimal paths selection: Among the many paths selected at the previous step, only a small proportion of them are within (or partially within) a crack. Such paths are expected to be made of pixels of darker intensities than the others, so we use again a threshold on the cost path to select the best

DETECTION BY SELECTION OF MINIMAL PATHS	
C1 - Endpoint selection \mathcal{E}	a) Select local lowest grey level pixels $\mathcal{M} = \{m_i \mid m_i = \operatorname{argmin}_{x \in I_P^i}(I(x))\}$ b) Evaluate threshold T_e c) Select $\mathcal{E} = \{e_i \in \mathcal{M} \mid I(e_i) \leq T_e\}$
C2 - Minimal path estimation p_{ij}	<u>For</u> each pair (e_i, e_j) with $e_i \in \mathcal{E}$, $e_j \in \mathcal{E}$ and $e_j \in \mathcal{V}(e_i)$ <u>Do</u> Estimate minimal path p_{ij} with its cost $c(p_{ij})$
C3 - Minimal path selection \mathcal{S}	a) Evaluate threshold T_c b) Estimate skeleton \mathcal{S} $\{p_{ij} \mid c(p_{ij}) \leq T_c\}$
Notations	I_P^i : Sub-image i of size $P \times P$ $I(x)$: Grey level of pixel x $\mathcal{V}(a)$: Endpoint neighbors of a (maximum 8) p_{ij} : Minimal path from x_i to x_j with cost $c(p_{ij})$

Fig. 2. Pseudo-code of the three core steps of the proposed MPS algorithm.

candidate paths. Since the goal of this proposed step is to select paths with the lowest mean intensities and not the shortest ones, it is important to threshold the following normalised version of cost (2):

$$c(p_{ij}) = \frac{1}{\operatorname{card}(p_{ij})} \sum_{m=i}^j I(m), \quad (3)$$

where $\operatorname{card}(p_{ij})$ is the length of the path (in pixels). We have chosen $T_c = \mu_c - k_c\sigma_c$, where μ_c is the mean and σ_c is the standard deviation of the costs (see Subsection V-A for the choice for k_c). As shown on Fig. 1(C3), this step makes the result converge towards the skeleton of the crack, *i.e.*, a one pixel-wide estimation of the crack with some artefacts.

C. Post-processing steps

Two kinds of improvements can still be performed, see Fig. 3. On the one hand, some paths or some parts of the paths correspond to false detections. On the other hand, the width of the crack has to be evaluated.

P1) Elimination of artefacts: Some small isolated paths may be present in the estimated crack, due to the texture of the road. A simple operation is to introduce a new threshold T_s on the minimal size of a path. The value of T_s can be empirically tuned, as shown in Subsection V-A.

Moreover, for some of the paths that constitute the crack skeleton, a frequent situation is that only one endpoint actually belongs to the crack. The resulting path is then partly inside the crack, and partly outside. The outside part forms a spurious “spike”. When several spikes share a common endpoint outside the crack, they form a “loop”. Both spikes and loops correspond to false positive pixels and must be eliminated. To

P1 – Skeleton refinement \mathcal{S}

- a) Remove small isolated paths
 - i) Evaluate threshold T_s
 - ii) Refine $\mathcal{S} = \{p_{ij} \in \mathcal{S} \mid \text{card}(p_{ij}) \leq T_s\}$
- b) Remove spikes and loops
 - i) Find extremities and junctions e_i^m
 - ii) Readjust paths p_{ij} between (e_i^m, e_j^m) with $e_j^m \in \mathcal{V}(e_i^m)$
 - iii) Compute new costs $c(p_{ij})$
 - iv) Refine $\mathcal{S} = \{p_{ij} \in \mathcal{S} \mid c(p_{ij}) \leq T_c\}$

P2 – Width detection

- a) Evaluate threshold T_w
- b) Repeat
 - i) Select $\mathcal{S}_v = \{v_i \in \mathcal{V}(\mathcal{S}) \mid I(v_i) \leq T_w\}$
 - ii) $\mathcal{S} = \mathcal{S} \cup \mathcal{S}_v$
- Until \mathcal{S} is unchanged

Notations, cf. Fig. 2.

$\mathcal{V}(\mathcal{S})$: Neighbours of skeleton \mathcal{S} (8-connectivity)

Fig. 3. Pseudo-code of the two post-processing steps.

do so, we first divide the skeleton into linear segments, such that both extremities of each segment are either a junction point, or an extremity of the crack itself. For example, a crack having the shape of letters A, H and P would be cut into four, five and three segments, respectively. The interest of such a partitioning step is to isolate the spikes and the spurious parts of loops into segments of higher average intensity than that of the “good” segments. A new thresholding operation is then performed on each segment, using the same threshold T_c as in Step C3.

P2) Width detection: The proposed width detection procedure consists in absorbing dark pixels neighboring the currently detected crack, according to a threshold test. The adopted threshold parameter is $T_w = \mu_w + k_w \sigma_w$, where μ_w and σ_w are the mean and the standard deviation of the grey levels within the currently detected crack, see Subsection V-A for the choice for k_w . The aggregation process is performed iteratively, so that several “layers” of dark pixels may be incorporated.

IV. ASSESSMENT PROTOCOL

In Section V, the proposed MPS algorithm will be tested both on a synthetic image, and on five real image databases. The test images are presented in Subsection IV-A. The performance of five existing methods will be also presented for comparison purposes. In real data cases, the definition of objective evaluation criteria is not an easy task. In Subsection IV-B, we propose a semi-automatic way of generating reference segmentation results, *i.e.*, a pseudo ground truth. Finally, Subsection IV-C introduces performance indices to evaluate

the mismatch between the reference result and the output of any segmentation method.

A. Tested dataset

The dataset is composed of one simulated and of 269 real images. The synthetic image allows to test the behavior of the MPS algorithm in a fully controlled framework, while real ones allow to evaluate the algorithm in a realistic context.

The simulated image of size 256×256 pixels contains some artificial crack patterns that have been superimposed to a real image of pavement texture. The simulated cracks have chaotic angular variations, with some ramifications and two thickness values (one and two pixels), as shown on the upper part of Fig. 11. Moreover, the grey level distribution of the pixels within the cracks has been chosen in conformity with the one empirically identified on a real image. In particular, the grey level distributions of the two pixel categories, namely the crack and the background pixels, significantly overlap.

The chosen 269 real images are expected to form a representative set of samples in terms of pavement texture and of crack patterns, with ramifications at some places and varying thickness along the crack. They can be decomposed in two categories: 68 images with reference segmentations (details about these reference segmentations are given in the next section) and 201 images without reference segmentation. Initially, we collected 62 images from one sensor, the Aigle-RN system presented in Fig. 4, and we computed a reference segmentation for 38 images from this database. Thanks to the Framework Program for European Research and Technological Development, called TRIMM for Tomorrows Road Infrastructure Monitoring and Management [?], we obtained 207 additional images acquired with four other sensors. It is obviously difficult and expensive to obtain a reference segmentation for quantitative evaluation on such a large dataset. In practice, we generated a reference segmentation for only 30 representative images from these 4 additional databases.

For all the systems tested, the acquisition are made perpendicular to the road, which means that the optical axis of the sensor is perpendicular to the road. One of these systems, named ESAR, corresponds to a static acquisition (not on a vehicle) with no controlled lighting and the four others are dynamic ones (on a vehicle) with controlled lighting. While the system Aigle-RN uses stroboscopic lights, laser is used by the three remaining ones, namely Tempest 2¹, LCMS² and LRIS³. More details about the sensors and the tested images are given In table I.

For the sake of clarity, let us divide the 269 images in three sets:

- **Dataset 1** contains the 38 images with reference segmentations acquired by Aigle-RN system. These images have been collected at traffic speed for periodically monitoring the French pavement surface condition. They have been pre-processed to mitigate the influence of non-uniform lighting conditions.

¹<http://yotta.co.uk>

²<http://www.pavometrics.com/en/lcms.html>

³<http://www.pavometrics.com/en/lris.html>



Fig. 4. The acquisition system used for the acquisition of the 38 images of dataset 1 – It is based on three sensors and the processing is done 1 meter by 1 meter with no overlap.

- **Dataset 2** contains 30 images acquired by the other four systems, with reference segmentations.
- **Dataset 3** corresponds to the remaining 201 images without reference segmentations. This last dataset allows only visual evaluations and comparisons.

SYSTEM	NB. OF IMAGES	LIGHTING SYSTEMS	ACQUISITION	IMAGE
Aigle-RN	62 (38)	Stroboscopic lights	Dynamic	
ESAR	30 (15)	Uncontrolled lighting	Static	
LCMS	65 (5)	Laser	Dynamic	
LRIS	89 (3)	Laser	Dynamic	
Tempest 2	23 (7)	Laser	Dynamic	

TABLE I

PRESENTATION OF THE 269 IMAGES TESTED FOR EACH SENSOR. THE NUMBER OF IMAGES WITH PGT IS INDICATED BETWEEN BRACKETS.

B. Pixel-based ground truth

In the synthetic data case, the ground truth can be defined in an unambiguous manner at the pixel level. The situation is more complex in real data cases. First of all, it is almost impossible to guarantee any ground truth in a realistic context. The best that we can obtain is a reference as reliable as possible. Even a complete manual segmentation is not as reliable as expected [10]. In the latter reference, a pseudo ground truth (PGT) is defined as the fusion of the manual segmentations obtained by four different experts. Here, we rather introduce a semi-automatic segmentation that involves only one human operator whose main role is to select pairs of pixels considered as endpoints of a crack segment. We suppose that manual selection of endpoints is enough reliable. Then, we know that Dijkstra algorithm guarantees the estimation of the minimal path between two points. It can be erroneous only if we have a false minimal path (due to texture) that intersects with the crack, in such a case the wrongly estimated part

can be removed manually. According to our own experience, such a semi-automatic procedure is quite fast and reliable. Furthermore, the post-processing step P2 is applied to estimate the thickness of the crack and to provide the whole crack pattern.

C. Evaluation criteria

When comparing segmentation results and the ground truth or the PGT, the following four pixel categories are considered:

- true positives (TP) correspond to correct detection of pixels belonging to the crack structure;
- false positives (FP) are wrongly detected crack pixels (*i.e.*, false alarms);
- false negatives (FN) are crack pixels that have been missed by the detection process;
- true negatives (TN) are background pixels that are correctly labelled by the detection process;

The number of pixels falling in each category is commonly used to quantify the agreement between detection and ground truth. Several indices can be deduced from the four basic figures, among which the following ones are widely used [32]:

- The Precision index highlights the proportion of false alarms:

$$P = \frac{TP}{TP + FP}.$$

- The Sensitivity index highlights the proportion of non-detected pixels.

$$S = \frac{TP}{TP + FN}.$$

- The DICE Similarity Coefficient (DSC) is the harmonic mean of precision and sensitivity:

$$DSC = \frac{2TP}{2TP + FP + FN}. \quad (4)$$

The DICE coefficient (4) combines the results of the first two criteria and it is commonly used as a global quality measure. It puts emphasize on good detections TP as a function of wrong decisions. Besides, it is especially suited when pixels to be detected are weakly represented, which is the case here. In the case of a perfect detection, we have $DSC = 1$, while $DSC = 0$ corresponds to a totally erroneous decision. In practice, it has been argued that a DSC value beyond 0.7 indicates an excellent agreement [33].

Finally, considering that the generation of a faithful PGT remains a difficult task for many real images, we propose to tolerate a small distance between the detection and the reference segmentation for the calculation of the TP rate. Then, it means that TP pixels are included within a 2 pixel vicinity of the PGT.

D. Comparison of methods

Very few comparative study between automatic pavement crack detection methods can be found in the literature. One difficulty is that several reference methods are protected commercial products, and their description is not publicly available. Here, we propose a partial comparison involving

five existing segmentation methods, that can be grouped into two families.

- **Modelling based methods** are composed of a photometric criterion (cracks pixels are darker than other pixels) and a local geometric criterion (locally, a crack can be considered as a small segment).

- M1 [34] consists in enhancing the contrast with adaptive 2D filtering in a multi-scale manner and in four different directions. Then, segmentation is done with a Markovian modelling where manipulated elements (sites) correspond to 3×3 blocks. Four possible configurations are distinguished (four segments in four directions). The segmentation results at all levels are then merged to compute the final result.
- M2 [10] is an improved variant of [34] where more configurations are proposed (sixteen) in order to better cover all the real local configurations of sites in the neighborhood.

- **Minimal path methods** are closer to the one introduced in this paper. Such methods are based on finding minimal paths between endpoints.

- GC is a Geodesic Contour method [20] with automatic selection of points of interest based on autocorrelation.
- FFA, Free Form Anisotropy, method [21], [?] is based on the estimation of minimal paths of a given length, d , at each pixel in four directions. Each current pixel is considered to belong to a crack when the path cost strongly varies with the direction.
- MPS0 [22] is a previous version of the Minimal Path Selection (MPS) method.

For FFA approach, an important parameter corresponds to the maximal length of the minimal paths, d . [?] indicates that “The distance must be higher than granule size to obtain an efficient filtering. If distance d is high enough, there is no noise detection”. Here, the chosen value $d = 30$ fulfills this criterion on dataset 1, in the sense that significantly lower values of d introduce wrong detections due to the pavement texture. For the four methods M1, M2, GC and MPS0 previously introduced, all the parameters used are fixed as recommended in each associated publication.

V. PERFORMANCE STUDY

A. Parameter setting

In practice, the proposed MPS algorithm requires the tuning of five parameters: the size of the image subsets P for local image analysis (Step C1), and the thresholds T_e (Step C1), T_c (Step C2), T_s (Step P1) and T_w (Step P2).

The value of P must not be too large to limit the computation time of the Dijkstra algorithm (since the latter is quickly growing with the distance between endpoints). Fig 5 shows an example. However, a small value of P can have an influence on the detection performance, as illustrated by Fig. 6. In fact, the choice has an impact essentially on the computing time while the quantitative results remain essentially similar for all the P values. Let us remark that such a choice is not very

different to the block size value adopted for other block-based approaches, *i.e.*, between 7 and 9 in [35], [36].

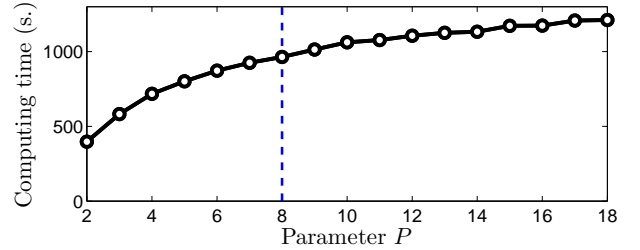


Fig. 5. Computation time as a function of the value of the window size P , for dataset 1.

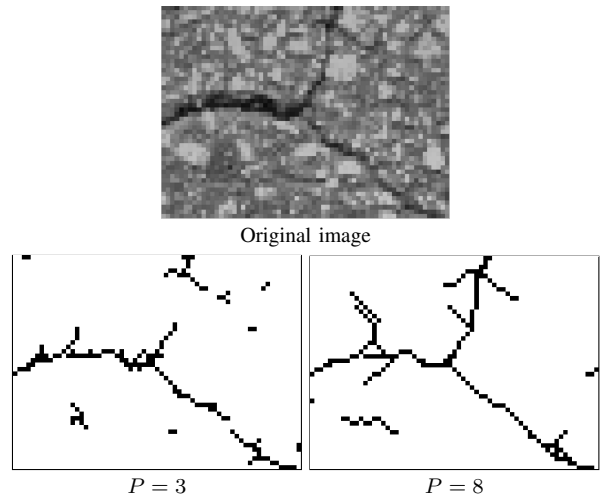


Fig. 6. Influence of parameter P on the detected paths. For small values of P such as $P = 3$, some parts of the cracks become disconnected.

The choice of k_e determines the threshold value $T_e = \mu - k_e\sigma$ that allows to retain only the darkest endpoints. Smaller values of k_e lead to discard only few endpoints, so the following steps become more computationally demanding. Larger ones eliminate more pixels, with the risk to remove crack pixels (see Fig. 7 for an illustration). In practice, we have found that $k_e = 1$ corresponds to a suited value. However, when this parameter value varies between 0 and 2, the percentage of TP varies only between 3.8 and 4.2. Again, this choice has mostly an impact on the computing time.

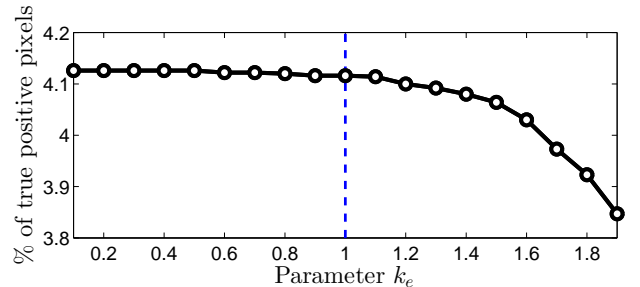


Fig. 7. Percentage of TP among the endpoints as a function of parameter k_e for datasets 1 and 2. For the chosen value of $k_e = 1$, 6% of the endpoints are removed.

The choice of k_c determines the threshold value $T_c = \mu_c - k_c\sigma_c$ that allows to retain only the paths of lowest costs among the ones found at Step C2. This parameter is a crucial one but its value is quite easy to choose. In fact, the results presented in Fig. 8 highlight that the value of k_c corresponds to a trade-off between precision and sensitivity. Beyond $k_c = 2$, the sensitivity becomes too low. We have chosen to retain the intermediate value $k_c = 1$, so that both thresholds T_e and T_c correspond to a unit standard deviation from the corresponding means.

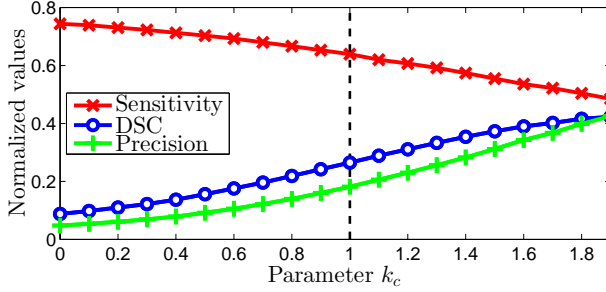


Fig. 8. Precision, sensitivity and DSC value variations with respect to parameter k_c for datasets 1 and 2.

As concerns the threshold T_s , Fig. 9 indicates that the value $T_s = 60$ empirically corresponds to a good trade-off to improve the precision without loosing much sensitivity. This parameter is also crucial. We have chosen its value given that road cracks that are lower than 10cm are usually not considered as significant. Such a choice is coherent for an image resolution of 1mm per pixel and should be adapted to a different resolution (or to a different goal in term of size of detected cracks).

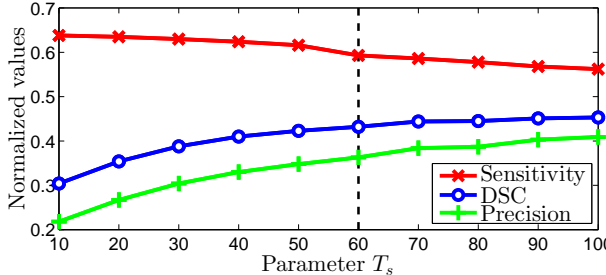


Fig. 9. Precision, sensitivity and DSC value variations with respect to parameter T_s for datasets 1 and 2.

Finally, the choice of k_w determines the threshold value $T_w = \mu_w + k_w\sigma_w$ to merge some dark pixels neighboring the currently detected crack structure. An appropriate value for k_w should increase the sensitivity with a low impact on the precision. According to Fig. 10, there is no doubt that $k_w = 0.6$ is the best choice, since it corresponds to the maximal value of DSC. We can also notice that for $k_w > 0.6$, the DSC value is quite stable.

B. Evaluations and comparisons on simulated data

According to Fig. 11 and 12, the results obtained by the two Markov-based methods M1 and M2 are very sensitive to

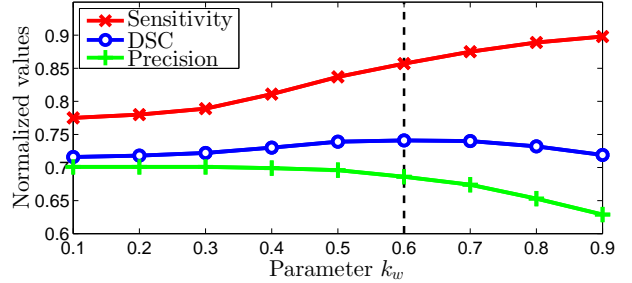


Fig. 10. Precision, sensitivity and DSC value variations with respect to parameter k_w for datasets 1 and 2.

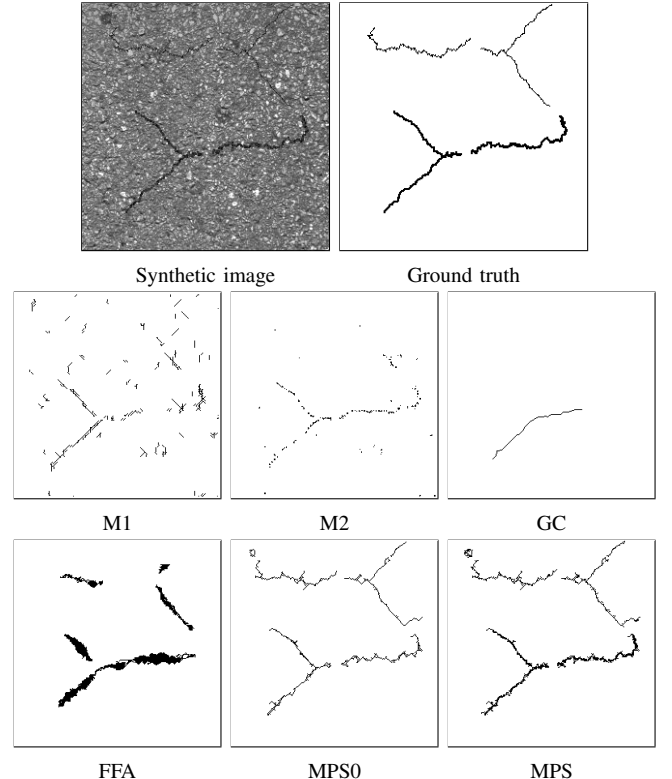


Fig. 11. Segmentation results on a synthetic image for the six methods compared to the ground truth.

the image texture. The performance of GC strongly depends on the automatic determination of the points of interest. In this synthetic image, since many points of interest have been detected only on a small part of the cracks, the method produces a high rate of FN. On the contrary, the FFA method detects a continuous crack path. However, the directional and length constraints clearly prevent the method from detecting the chaotic crack pattern and the fine structure of the crack. For instance, the direction change is missed at the right hand extremity of the thicker crack. The MPS0 method shows better performance compared to the first three methods. Nonetheless, some loop artefacts limit its performance to 0.75 in terms of DSC value. MPS broadly outperforms the other tested methods, with a DSC value of 0.83. A closer look at the result displayed at Fig. 11 confirms that MPS accurately detects cracks of any form and thickness.

To sum up, GC shows the lowest performance on the

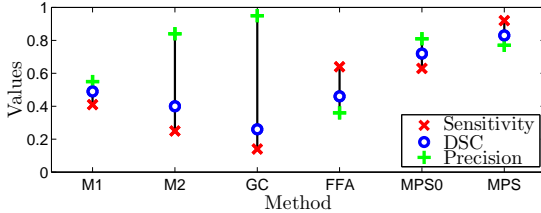


Fig. 12. Precision, sensitivity and DSC values for the six different methods applied to the synthetic image on Fig. 11.

tested synthetic image. FFA, M1 and M2 provide intermediate results, and the two MPS methods yield the best overall performance, the new version being superior to the previous one.

C. Performance comparison on images from the real datasets

Here, the performance of the six methods are evaluated on the images of the real datasets 1 and 2 introduced in Subsection IV-A. First, an image sample from dataset 1 is used to illustrate some qualitative aspects of the comparison but the results on all the datasets are resumed in Fig. 14.

According to Fig. 13, the Markov-based methods provide discontinuous crack segmentation, owing to the sensitivity to the image texture. M2 also detects a lot of small FP within the image background, including the two dark small patches at the bottom. GC gives the worst performance, because only a small part of the crack has been detected. The FFA method detects a more continuous crack path than M2 and HA. The segmented result appears as a thick line, implying a lot of FP within the vicinity of the crack pattern. At some places, the crack pattern is scattered in small pieces and FN pixels appear. As opposed to the latter, MPS accurately reveals the thin and chaotic structure of the whole crack pattern with reduced artefacts. The overall performance of the six methods on datasets 1 and 2 are shown on Fig. 14 and 15, respectively.

For dataset 1, the two Markov-based methods depict sensitivity, precision and DSC criteria below 0.5 because of high FP and FN rates. The GC method presents a high precision level, owing to a small amount of FP pixels, but as a counterpart, its sensitivity and DSC values are very low due to the large number of FN. As opposed to the latter, FFA method provides a smaller amount of FN pixels and a larger number of FP pixels in the vicinity of the cracks, which results in a small precision level, a rather high sensitivity, and only a moderate DSC value. The two MPS methods yield by far the best average performance in terms of sensitivity, precision and DSC. Once again, MPS provides a significant improvement over MPS0, meaning that the estimation of thickness has significantly improved the segmentation result.

The overall performance on dataset 2 are under the overall performance of the first dataset. However, the same remarks can be done and the MPS approach still gives the best results.

As a conclusion, the average results obtained on the real image datasets confirm the conclusion drawn on the simulated case: MPS is the most accurate method, followed by MPS0, FFA, M1, M2, and GC in descending order of performance.

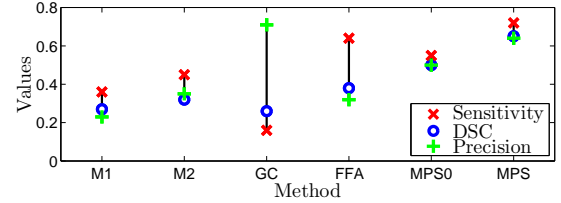


Fig. 14. Averaged values of precision, sensitivity, and DSC for the 38 real images of the data set 1.

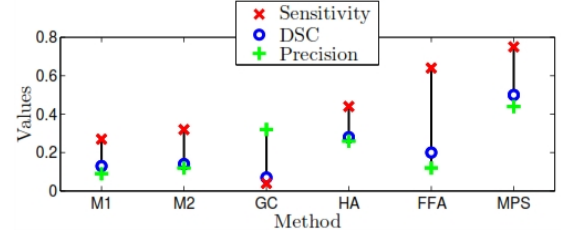


Fig. 15. Averaged values of precision, sensitivity, and DSC for the 30 real images of dataset 2. This dataset is more difficult than the French one because it contains images from different sensors with high variability in the lighting and different problems in the images, like textures or other defaults that are comparable to cracks and low contrast. The methods M1, M2 and GC are not able to detect the cracks and their performances are under the performances of HA. Again, the proposed approach obtained the best results for each criterion.

Another test consists in evaluating the sensitivity of the MPS method to the image texture. The latter may depend on the pavement materials owing to either the size or the colour of aggregates, on the light scattering over the pavement roughness, or on the wearing of the road surface which modifies the material granularity at some places of the pavement. Here, three different images have been selected within the real datasets, of growing difficulty from Image A to Image C, the latter being the most textured, see Fig. 16. MPS performs well on Images A and B, which is confirmed by a high DSC value, see Table 16. In the case of Image C, MPS produces a coherent result, but it corresponds to a more continuous crack than the one produced by the expert in the PGT image. This explains why the obtained DSC value is low.

Table II also gathers the performance of the other five methods on the same three images. For all methods, the smallest DSC value is reached for the most textured image, namely Image C, while MPS produces the highest DSC value for the three images.

Method	M1	M2	GC	FFA	MPS0	MPS
Image A	0.35	0.37	0.24	0.44	0.58	0.77
Image B	0.18	0.28	0.42	0.37	0.37	0.75
Image C	0.06	0.18	0.00	0.24	0.18	0.32

TABLE II
DSC VALUES FOR THE SIX DIFFERENT METHODS APPLIED TO THE THREE IMAGES OF FIG. 16.

Finally, the images without a PGT (i.e., dataset 3) have been processed. The results visually confirm that MPS provides far more precise detections than the other methods. The whole set of results are available from the following web page:

http://www.irit.fr/~Sylvie.Chambon/Crack_Detection_Database.html.

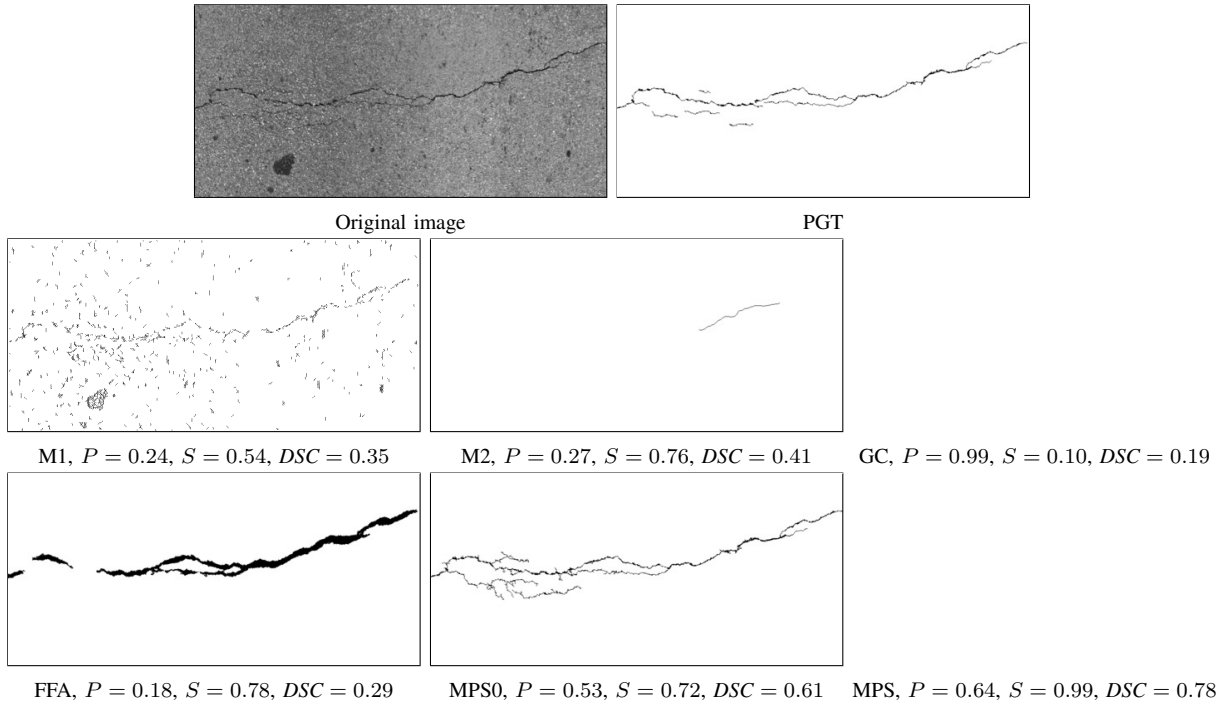


Fig. 13. An example of outcome from the six different methods compared to the PGT.

Some of these results can also be found in [?].

VI. CONCLUSION AND PERSPECTIVES

Our main contribution is an improved minimal path selection method based on the appropriate selection of minimal paths between endpoints. Compared to our initial version of [22], it incorporates a refined artefact filtering step and enables the estimation of the thickness of the crack pattern. A complete evaluation protocol has been introduced on both synthetic and real images (from five different sensors). The comparison with five existing methods has shown that the proposed method affords the best DSC rate. To our best knowledge, such a kind of precise and complete evaluation is quite new in this context. In the future, it could provide a basis for additional comparisons involving new methods. It can be argued that the assessment protocol provides a bias in favour of the MPS method because the same algorithm, namely Dijkstra, is used to process the image and to provide the PGT. Indeed, the best performance achieved by MPS on simulated data and the coherency between the MPS results on simulated and real data sets have contributed to remove the latter ambiguity. In conclusion, the proposed method provides very robust and precise results in a wide range of situations, in a fully unsupervised manner, which is beyond the current state-of-the-art.

One of our main perspectives will be to reduce the computation time of the method by GPU, Graphics Processing Unit, programming, especially at step III-B of the algorithm in Fig. 2. We could also obtain a faster version by replacing the exact Dijkstra algorithm by a suboptimal version in the A* family [37]. Finally, 3D imaging systems are of growing use and give the potential to improve crack detection [2]. It is believed that the MPS relies on a versatile principle and

thus may cope with the elevation data which is available from these latest imaging technologies.

REFERENCES

- [1] M. Ahmed and C. Haas, "The potential of low cost close range photogrammetry towards unified automatic pavement distress surveying," in *Transportation Research Board Meeting*, 2009.
- [2] M. Gavilán, D. Balcones, O. Marcos, D. F. Llorca, M. A. Sotelo, I. Parra, M. Ocaña, P. Aliseda, P. Yarza, and A. Amírola, "Adaptive road crack detection system by pavement classification," *Sensors*, pp. 9628–9657, 2011.
- [3] H. Oliveira and P. L. Correia, "Automatic road crack detection and characterization," *IEEE Trans. on Intelligent Transportation Systems*, vol. 14, no. 1, pp. 155–168, 2013.
- [4] J. J. Acosta, L. Adolfo, and R. L. Mullen, "Low-cost video image processing system for evaluating pavement surface distress," *Journal of the Transportation Research Board*, vol. 1348, pp. 63–72, 1992.
- [5] J. Tang and Y. Gu, "Automatic crack detection and segmentation using a hybrid algorithm for road distress analysis," in *IEEE Trans. on Systems, Man and Cybernetics*, 2013, pp. 3026–3030.
- [6] Y. Hu and C. Zhao, "A local binary pattern based methods for pavement crack detection," *Journal of Pattern Recognition Research*, , no. 1, pp. 140–147, 2010.
- [7] N. Otsu, "A threshold selection method from gray-level histograms," *IEEE Trans. on Systems, Man and Cybernetics*, vol. 9, no. 1, pp. 62–66, 1979.
- [8] H. Cheng, J. Chen, C. Glazier, and Y. Hu, "Novel approach to pavement cracking detection based on fuzzy set theory," *Journal of Computing in Civil Engineering*, vol. 13, no. 4, pp. 270–280, 1999.
- [9] T. Tomikawa, "A study of road crack detection by the meta-genetic algorithm," in *IEEE Africon*, 1999, vol. 1, pp. 543–548.
- [10] S. Chambon and J.-M. Molliard, "Automatic road pavement assessment with image processing: Review and comparison," *Int. Journal of Geophysics*, p. ID 989354, 2011.
- [11] J. Bray, B. Verma, Xue Li, and Wade He, "A neural network based technique for automatic classification of road cracks," in *Int. Joint Conf. on Neural Networks*, 2006, pp. 907–912.
- [12] H. Oliveira and P. L. Correia, "Supervised strategies for cracks detection in images of road pavement flexible surfaces," in *European Signal Processing Conf.*, 2008.

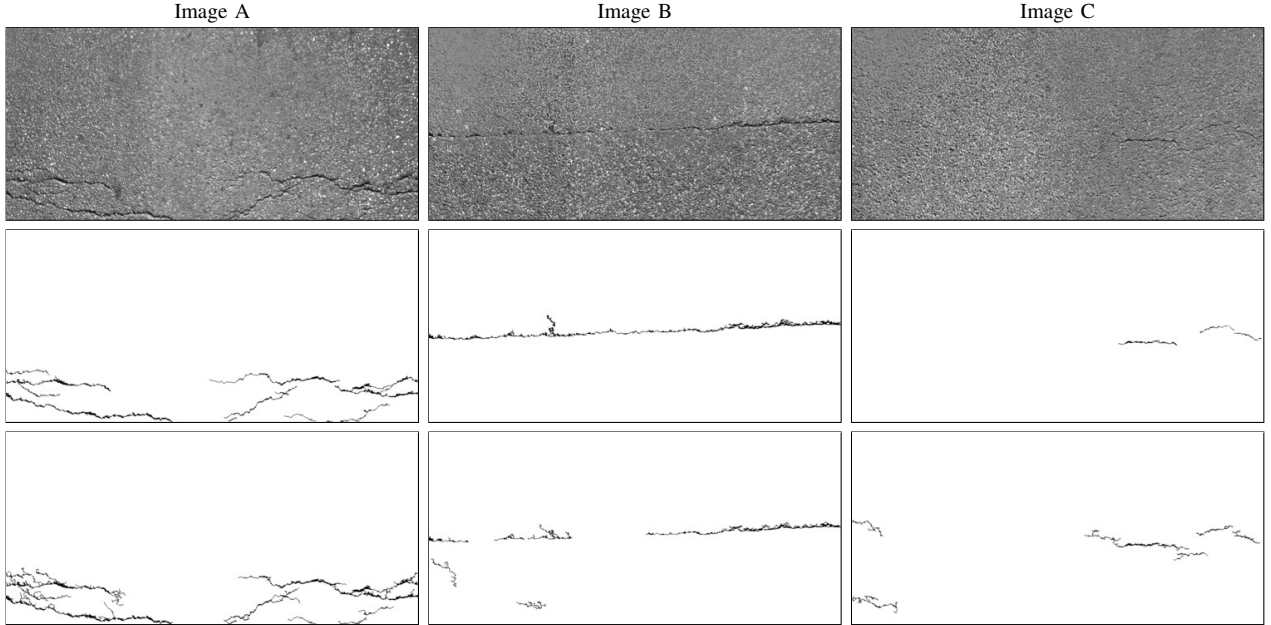


Fig. 16. MPS results on three real images of varying textures. The second and third lines respectively show the PGT and the results obtained by MPS.

- [13] A. Cord and S. Chambon, "Automatic road defect detection by textural pattern recognition based on adaboost," *Computer-Aided Civil and Infrastructure Engineering*, vol. 27, no. 4, pp. 244–249, 2011.
- [14] H. N. Koutsopoulos and A. B. Downey, "Primitive-based classification of pavement cracking images," *Journal of Transportation Engineering*, vol. 119, no. 3, pp. 402–418, 1993.
- [15] N. Tanaka and K. Uematsu, "A crack detection method in road surface images using morphology," in *Workshop on Machine Vision Applications*, 1998, pp. 154–157.
- [16] N. Coudray, A. Karathanou, and S. Chambon, "Multi-resolution approach for fine structure extraction - application and validation on road images," in *Int. Conf. on Computer Vision Theory and Applications*, 2010, pp. 142–147.
- [17] P. Subirats, O. Fabre, J. Dumoulin, V. Legeay, and D. Barba, "Automation of pavement surface crack detection with a matched filtering to define the mother wavelet function used," in *European Signal Processing Conf.*, 2006.
- [18] P. Delagnes and D. Barba, "A markov random field for rectilinear structure extraction in pavement distress image analysis," in *Int. Conf. on Image Processing*, 1995, vol. 1, pp. 446–449.
- [19] Q. Zou, Y. Cao, Q. Li, Q. Mao, and S. Wang, "Cracktree: Automatic crack detection from pavement images," *Pattern Recognition Letters*, vol. 33, no. 3, 2012.
- [20] S. Chambon, "Detection of points of interest for geodesic contours: Application on road images for crack detection," in *Int. Conf. on Computer Vision Theory and Applications*, 2011.
- [21] T. S. Nguyen, S. Begot, F. Duculty, and M. Avila, "Free-form anisotropy: A new method for crack detection on pavement surface images," in *Int. Conf. on Image Processing*, 2011, pp. 1069–1072.
- [22] R. Amhaz, S. Chambon, J. Idier, and V. Baltazard, "A new minimal path selection algorithm for automatic crack detection on pavement images," in *Int. Conf. on Image Processing*, 2014.
- [23] V. Kaul, A. Yezzi, and Y. Tsai, "Detecting curves with unknown endpoints and arbitrary topology using minimal paths," in *IEEE Trans. on Pattern Analysis and Machine Intelligence*, 2012, vol. 34, pp. 1952–1965.
- [24] J. Mille, S. Bougleux, and L. Cohen, "Minimally overlapping paths sets for closed contour extraction," in *Int. Conf. on Computer Vision Theory and Applications*, 2012.
- [25] E. W. Dijkstra, "A note on two problems in connexion with graphs," *Numerische Mathematik*, vol. 1, no. 1, pp. 269–271, 1959.
- [26] J. A. Sethian, "A fast marching level set method for monotonically advancing fronts," in *Proceedings of the National Academy of Science*, 1995, pp. 1591–1595.
- [27] C. Sun and B. Appleton, "Multiple paths extraction in images using a constrained expanded trellis," *IEEE Trans. on Pattern Analysis and Machine Intelligence*, vol. 27, pp. 1923–1933, 2005.
- [28] T. Deschamps and L. Cohen, "Fast extraction of minimal paths in 3D images and applications to virtual endoscopy," in *Medical Image Analysis*, 2001, pp. 281–299.
- [29] L. D. Cohen and R. Kimmel, "Global minimum for active contour models: A minimal path approach," *Int. Journal of Computer Vision*, vol. 24, no. 1, pp. 57–78, 1996.
- [30] P. Yan and A. A. Kassim, "Medical image segmentation using minimal path deformable models with implicit shape priors," *IEEE Trans. on Information Technology in Biomedicine*, vol. 10, no. 4, pp. 677–684, 2006.
- [31] M. Kass, A. Witkin, and D. Terzopoulos, "Snakes : Active contour models," *Int. Journal of Computer Vision*, vol. 1, no. 4, pp. 321–331, 1988.
- [32] M. P. Sampat, Z. Wang, S. Gupta, A. C. Bovik, and M. K. Markey, "Complex wavelet structural similarity: A new image similarity index," *IEEE Trans. on Image Processing*, vol. 18, no. 11, pp. 2385–2401, 2009.
- [33] A. P. Zijdenbos, B. M. Dawant, R. A. Margolin, and A. C. Palmer, "Morphometric analysis of white matter lesions in mr images: method and validation," *IEEE Trans. on Medical Imaging*, vol. 13, no. 4, pp. 716–724, 1994.
- [34] S. Chambon, P. Subirats, and J. Dumoulin, "Introduction of a wavelet transform based on 2D matched filter in a markov random field for fine structure extraction: Application on road crack detection," in *IS&T/SPIE Electronic Imaging - Image Processing: Machine Vision Applications II*, 2009.
- [35] Y. Huang and B. Xu, "Automatic inspection of pavement cracking distress," *J. Electronic Imaging*, 2006.
- [36] Z. Li and X. Zou, "Skeleton detection of crack based on multiscale geometric analysis in space domain," in *Int. Conf. on Automatic Control and Artificial Intelligence*, 2012, pp. 1862–1865.
- [37] D. Delling, P. Sanders, D. Schultes, and D. Wagner, "Engineering route planning algorithms," *Algorithmics of large and complex networks*. Springer, Lecture Notes in Computer Science, vol. Volume 5515, pp. 117–139, 2009.



Rabih Amhaz is currently a Ph.D. student in IFSTTAR (the French institute of science and technology for transport, development and networks) at Centrale Nantes. Working now in IRIT (Institut de Recherche en Informatique de Toulouse) of INP-ENSEEIHT, his research interest concerns crack segmentation using minimal path approach.



Sylvie Chambon received the Ph.D degree in Computer Science from the University of Toulouse, France, about "Colour stereoscopic matching with occlusions". From 2006 to 2007, she was a post-doctoral researcher at Télécom Paris in multi-modal registration of medical images. From 2008 to 2011, she was a permanent researcher IFSTTAR (the French institute of science and technology for transport, development and networks) and works on segmentation of thin structures and in particular, road cracks. Since September 2011, she is a assistant professor at INP-ENSEEIHT/IRIT and her research concerns matching, features detection and tracking, segmentation of thin structures and urban scenes.



Jérôme Idier was born in France in 1966. He received the Diploma degree in electrical engineering from Ecole Sup'erieure d'Electricité, Gif-sur-Yvette, France, in 1988, and the Ph.D. degree in physics from University of Paris-Sud, Orsay, France, in 1991. In 1991, he joined the Centre National de la Recherche Scientifique. He is currently a Senior Researcher with the Institut de Recherche en Communications et Cybernétique, Nantes, France. His major scientific interests are in signal and image processing, and more specifically in optimization and inference for inverse problems.

Dr. Idier is currently an elected member of the French National Committee for Scientific Research. He is also a member of the Signal Processing Theory and Methods Technical Committee of the IEEE Signal Processing Society.



Vincent Baltazard received the Ph.D. degree in signal processing from the University of Rennes, France, in 1994. From 1992 to 1993, he worked on ionospheric modeling and propagation at IPS Radio and Space Services, Sydney, Australia. From 1994 to 1996, he worked on microwave remote-sensing techniques at the Université Catholique de Louvain, Louvain-la-Neuve, Belgium. In 1996, he joined the Laboratoire Central des Ponts et Chaussées, France, as a researcher in the field of optical sensors. He is currently involved in nondestructive testing and evaluation techniques for civil engineering applications at IFSTTAR in Nantes.